Semester thesis

Characterization of microwave devices for multiplexing qubit readout

Author:
Patrik Caspar

Supervisor:
Dr. Mintu Mondal

ETH Zürich

Quantum Device Lab

Prof. Dr. Andreas Wallraff

July 20, 2015

Abstract

In this thesis work, properties of superconducting microwave circuits are investigated. Different microwave circuits consisting of coupled resonators are characterized by dipstick measurement in liquid helium and are also simulated using *Microwave Office*. Based on this study, a new design of microwave circuit involving 8 qubits has been proposed and possible required improvements are discussed. In this proposed design, the coupling capacitances between the readout resonator and the transmission line are determined to have desired coupling strengths. This study will help to improve the multiplexing readout technique involving many qubits.

Contents

1 Introduction

In the last few decades, the field of quantum information processing has grown significantly, on the theoretical as well as on the experimental side. Several physical implementations of quantum two level states have been pursued [6]. One approach is the superconducting qubit, which is a solid state artificial system implemented with superconducting electronic circuits, a field known as circuit quantum electrodynamics (cQED) [3]. In this context, on-chip microwave resonators are an important ingredient to build these superconducting electronic circuits. Coplanar waveguide (CPW) resonators can now be designed and fabricated with high quality factors and the resonance frequency can be controlled [2, 3]. By capacitively coupling to a transmission line, superconducting microwave resonators can be used for qubit readout. To build more complex on-chip circuits with several qubits, an efficient way of qubit readout is needed. In this thesis, the fundamental properties of superconducting resonators and their behaviour under capacitively coupling are studied.

To get a multiplexing readout design, the resonators have to be engineered properly. The most important parameter to reach reasonable fast measurements is the resonator coupling strength κ, which is mainly influenced by the coupling capacitance C_κ. In order to understand the underlying mechanisms, different devices are measured in an S-parameter measurement with a vector network analyzer. Furthermore, the behaviour of the designs under changes of the parameters are simulated with the software *AWR Microwave Office*. To compare the measurement and the simulation results with theory, a fit function for each design is derived and fitted to the data with *Mathematica*.

In the following, the theory needed to understand the main resonator properties and to derive the model fit functions is explained. Then the samples and measurement setup as well as simulation method are discussed in section 3, followed by the measurement and simulation results and discussion. The results consist mainly of data plots of transmission spectra received from the vector network analyzer and from simulation. Also the values for the extracted resonator properties such as quality factors, center frequencies and coupling strengths are shown. The main steps towards a multiplexing readout design are mentioned in section 5.

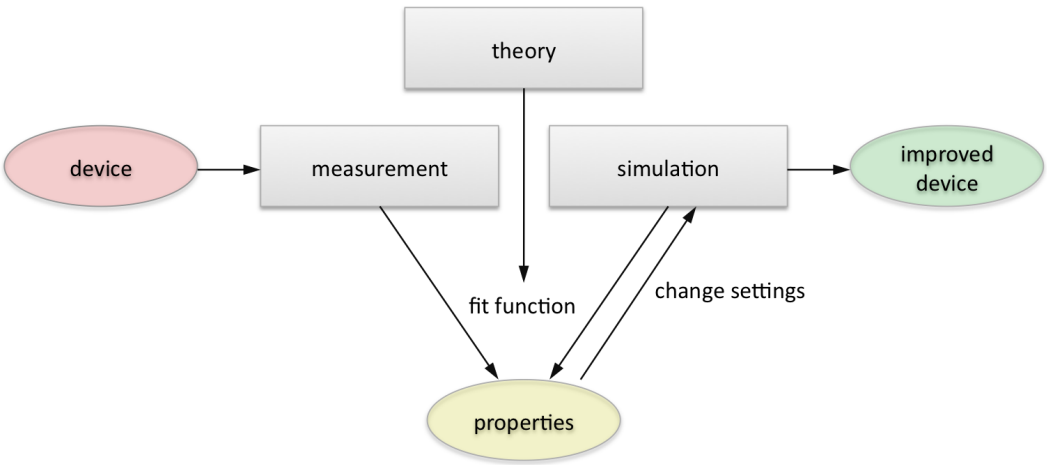

2 Theory

2.1 Coplanar waveguide resonator

The resonance frequency f_0 of a resonator is given by [3]:

$$f_0 = v_{\mathrm{ph}} \frac{1}{\lambda_0} = \frac{c}{\sqrt{\varepsilon_{\mathrm{eff}}}} \frac{1}{\lambda_0} = \frac{1}{\sqrt{L_l C_l}} \frac{1}{\lambda_0} \tag{1}$$

with the phase velocity v_{ph}, the wavelength of the fundamental resonator mode λ_0, the speed of light c, the capacitance per unit length C_l, the impedance per unit length L_l and the effective dielectric permittivity $\varepsilon_{\mathrm{eff}}$ which depends on the geometry as well as on the substrate.
The transmission through the resonator with resonance frequency $f_0 = \omega_0/2\pi$ can be described with a Lorentzian function with full width half maximum δf (adopted from [3]):

$$F_{\mathrm{Lorentz}}(f) = A_0 \frac{\delta f}{(f - f_0)^2 + \left(\frac{\delta f}{2}\right)^2} \tag{2}$$

An important characteristic of a resonator is the quality factor which is equal to 2π times the energy stored in the resonator divided by the energy dissipated per cycle. The loaded quality factor Q_{L} can be written in terms of the external quality factor Q_{ext} and the internal quality factor Q_{int} which is independent of the coupling.

$$\frac{1}{Q_{\mathrm{L}}} = \frac{1}{Q_{\mathrm{int}}} + \frac{1}{Q_{\mathrm{ext}}} \tag{3}$$

If the resonator is strongly coupled to the feed line, it is called overcoupled and $Q_{\mathrm{int}} \gg Q_{\mathrm{ext}}$. If otherwise the resonator is very weakly coupled, it is in the undercoupled regime with $Q_{\mathrm{int}} \ll Q_{\mathrm{ext}}$.

2.1.1 Half-wavelength resonator

A half-wavelength resonator is created by interrupting the CPW twice, which leads to a fundamental mode with a wavelength of twice the resonator length $l = \lambda_0/2$. The used coplanar waveguide resonators are described by the distributed element model, in which the capacitances C_l and inductances L_l are given per unit length. The center conductor with width W is separated from the ground planes by a gap of width S.

For asymmetrically coupled resonators the values in figure 2c and the quality factors are given in [9]:

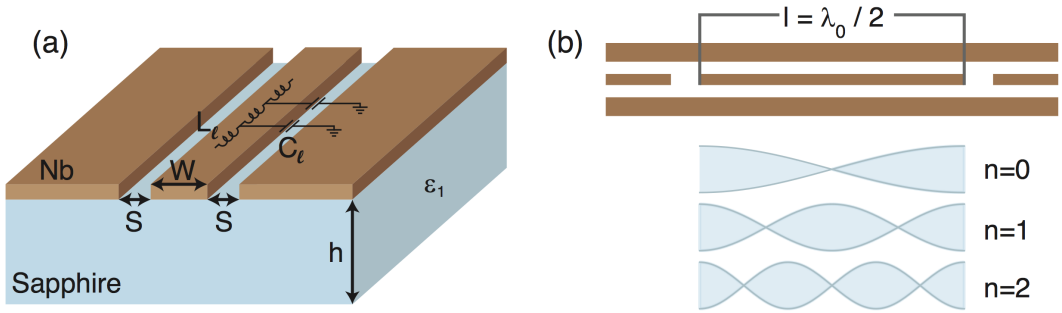

Figure 1: **Schematic from [9].** (a) Coplanar waveguide (CPW) from niobium on a sapphire substrate with dielectric permittivity ε_1. (b) Half-wavelength coplanar waveguide resonator with fundamental ($n = 0$) and higher modes ($n = 1, 2$).

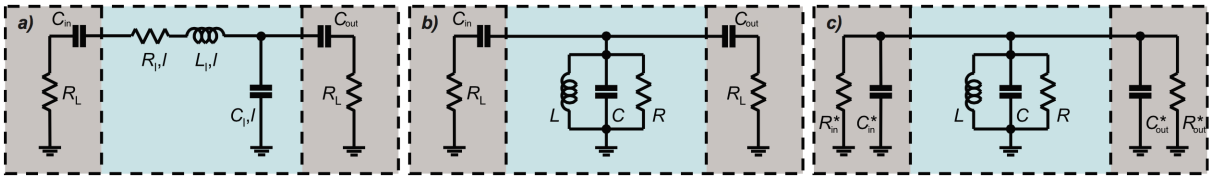

Figure 2: **Schematics of the resonator circuit from [3] with minor changes for asymmetric coupling.** (a) Distributed element representation of asymmetrically coupled transmission line (TL) resonator. (b) Parallel LCR oscillator representation of TL resonator. (c) Norton equivalent of asymmetrically coupled parallel LCR oscillator.

$$R^*_{\mathrm{in,out}} = \frac{1+\omega_0^2 R_\mathrm{L}^2 C_{\mathrm{in,out}}^2}{\omega_0^2 R_\mathrm{L} C_{\mathrm{in,out}}^2}, \quad C^*_{\mathrm{in,out}} = \frac{C_{\mathrm{in,out}}}{1+\omega_0^2 R_\mathrm{L}^2 C_{\mathrm{in,out}}^2}, \quad C = \frac{C_l l}{2}, \quad R = \frac{Z_0}{\alpha l} \tag{4}$$

$$\frac{1}{Q_\mathrm{L}} = \frac{\delta f}{f_0} = \underbrace{\frac{1}{\omega_0 C R}}_{1/Q_\mathrm{int}} + \underbrace{\frac{1}{\omega_0 C R^*_\mathrm{in}} + \frac{1}{\omega_0 C R^*_\mathrm{out}}}_{1/Q_\mathrm{ext}} \tag{5}$$

$$\Rightarrow Q_\mathrm{int} = \omega_0 R C = \frac{\pi}{2\alpha l} \tag{6}$$

$$\Rightarrow Q_\mathrm{ext} = \frac{1}{\omega_0^2 R_\mathrm{L}} \underbrace{\frac{\pi}{2Z_0}}_{\omega_0 C} \left(\frac{(1+\omega_0^2 R_\mathrm{L}^2 C_\mathrm{in}^2)(1+\omega_0^2 R_\mathrm{L}^2 C_\mathrm{out}^2)}{C_\mathrm{in}^2(1+\omega_0^2 R_\mathrm{L}^2 C_\mathrm{out}^2) + C_\mathrm{out}^2(1+\omega_0^2 R_\mathrm{L}^2 C_\mathrm{in}^2)} \right) \tag{7}$$

where ω_0 denotes the angular frequency of the fundamental mode, $R_\mathrm{L} = 50\,\Omega$ the load impedance, $Z_0 = \sqrt{L_l/C_l}$, α the attenuation constant, Q_L the loaded, Q_int the internal and Q_ext the external quality factor.

Now, the coupling strength κ can be calculated:

$$\kappa = \frac{\omega_0}{Q_\mathrm{L}} = \underbrace{\frac{2}{\pi}\omega_0 \alpha l}_{\omega_0/Q_\mathrm{int}} + \underbrace{\frac{2\omega_0^2 R_\mathrm{L}}{C_l l}\left(\frac{C_\mathrm{in}^2}{1+\omega_0^2 R_\mathrm{L}^2 C_\mathrm{in}^2} + \frac{C_\mathrm{out}^2}{1+\omega_0^2 R_\mathrm{L}^2 C_\mathrm{out}^2} \right)}_{\omega_0/Q_\mathrm{ext}} \tag{8}$$

For undercoupled resonators ($Q_\mathrm{int} \ll Q_\mathrm{ext}$) this leads to:

$$\kappa = \frac{\omega_0}{Q_\mathrm{L}} \approx \frac{\omega_0}{Q_\mathrm{int}} = \frac{2}{\pi}\omega_0 \alpha l \tag{9}$$

and for overcoupled resonators ($Q_\mathrm{int} \gg Q_\mathrm{ext}$):

$$\kappa = \frac{\omega_0}{Q_\mathrm{L}} \approx \frac{\omega_0}{Q_\mathrm{ext}} = \frac{2\omega_0^2 R_\mathrm{L}}{C_l l}\left(\frac{C_\mathrm{in}^2}{1+\omega_0^2 R_\mathrm{L}^2 C_\mathrm{in}^2} + \frac{C_\mathrm{out}^2}{1+\omega_0^2 R_\mathrm{L}^2 C_\mathrm{out}^2} \right) \tag{10}$$

2.1.2 Quarter-wavelength resonator

If the the CPW is interrupted at one side and shortened at the other side, a quarter-wavelength resonator is created with the property $l = \lambda_0/4$.

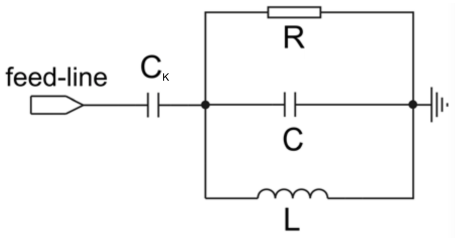

Figure 3: **Schematic from [4].** Lumped element equivalent circuit of a capacitive coupled quarter wavelength resonator.

For a quarter-wavelength resonator, the quality factor and κ can be derived using [4, 9]:

$$L = \frac{8l}{\pi^2}L_l, \quad L_l = \frac{R_\mathrm{L}\sqrt{\varepsilon_\mathrm{eff}}}{c}, \quad C = \frac{l}{2}C_l, \quad C_l = \frac{\varepsilon_\mathrm{eff}}{c^2 L_l}, \quad R = \frac{1}{\alpha l}R_\mathrm{L} \tag{11}$$

$$Q_\mathrm{int} = \omega_0 CR = \frac{\pi}{4\alpha l}, \quad Q_\mathrm{ext} = \omega_0 C_l l\left(\frac{1}{\omega_0^2 C_\kappa^2 R_\mathrm{L}} + R_\mathrm{L}\right) \tag{12}$$

$$\Rightarrow \kappa = \frac{\omega_0}{Q_\mathrm{L}} = \underbrace{\frac{4}{\pi}\omega_0\alpha l}_{\omega_0/Q_\mathrm{int}} + \underbrace{\frac{\omega_0^2 R_\mathrm{L}}{C_l l}\frac{C_\kappa^2}{1+\omega_0^2 C_\kappa^2 R_\mathrm{L}^2}}_{\omega_0/Q_\mathrm{ext}} \tag{13}$$

with the resonator length l, the inductance per unit length L_l, the capacitance per unit length C_l, the coupling capacitance C_κ, the effective dielectric permittivity ε_eff, the attenuation constant α and the load impedance $R_\mathrm{L} = 50\,\Omega$.

2.2 Input-output formalism

Since the input-output model is not only valid for lumped element resonators, but also for distributed element circuits such as transmission line resonators, it can be used to find fit functions for the investigated circuits. The following derivation is based on [8].

The equation of motion in the Heisenberg picture for a one sided cavity coupled to an external field is given by

$$\dot{A}(t) = -\frac{i}{\hbar}[A(t), H_\mathrm{sys}] - \frac{\kappa+\gamma}{2}A(t) + \sqrt{\kappa}a_\mathrm{in}(t) \tag{14}$$

and the time reversed equation by

$$\dot{A}(t) = -\frac{i}{\hbar}[A(t), H_\mathrm{sys}] + \frac{\kappa+\gamma}{2}A(t) - \sqrt{\kappa}a_\mathrm{out}(t) \tag{15}$$

which leads to the condition (for $\gamma \ll \kappa$)

$$a_\mathrm{in}(t) + a_\mathrm{out}(t) = \sqrt{\kappa}A(t) \tag{16}$$

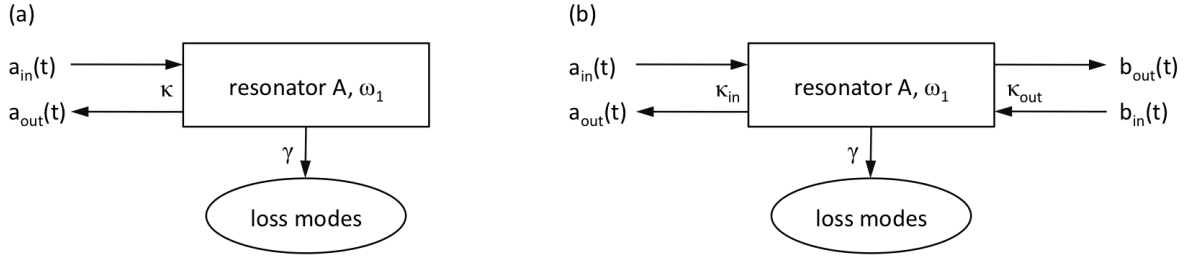

Figure 4: (a) One sided cavity. (b) Two sided cavity.

Here, $A(t)$ denotes the annihilation operator of the cavity field, $a_{\text{in,out}}(t)$ the annihilation operator of the input/output field, H_{sys} the system Hamiltonian as a function of the internal modes only, κ the coupling strength and γ the internal loss rate.

The system Hamiltonian corresponding to figure 4 is given by

$$H_{\text{sys}} = \hbar\omega_1 A^\dagger A \tag{17}$$

with the resonance frequency ω_1 of resonator A. Note the commutation relation $[A, A^\dagger] = 1$. In order to get algebraic equations, the Fourier transformation is applied:

$$A(t) = \frac{1}{\sqrt{2\pi}} \int_{-\infty}^{\infty} e^{-i\omega t} A(\omega) d\omega \tag{18}$$

which leads together with the Hamiltonian to the following equations for a one sided cavity:

$$\left(-i(\omega - \omega_1) + \frac{\kappa + \gamma}{2}\right) A(\omega) = \sqrt{\kappa} a_{\text{in}}(\omega) \tag{19a}$$

$$a_{\text{in}}(\omega) + a_{\text{out}}(\omega) = \sqrt{\kappa} A(\omega) \tag{19b}$$

For a two sided cavity, the derivation is similar and leads to the equations

$$\left(-i(\omega - \omega_1) + \frac{\kappa_{\text{in}} + \kappa_{\text{out}} + \gamma}{2}\right) A(\omega) = \sqrt{\kappa_{\text{in}}} a_{\text{in}}(\omega) + \sqrt{\kappa_{\text{out}}} b_{\text{in}}(\omega) \tag{20a}$$

$$a_{\text{in}}(\omega) + a_{\text{out}}(\omega) = \sqrt{\kappa_{\text{in}}} A(\omega) \tag{20b}$$

$$b_{\text{in}}(\omega) + b_{\text{out}}(\omega) = \sqrt{\kappa_{\text{out}}} A(\omega) \tag{20c}$$

To get the transmission function through a resonator out of this system of equations, the ratio $b_{\text{out}}(\omega)/a_{\text{in}}(\omega)$ has to be calculated. Since in the transmission measurement only $a_{\text{in}}(\omega)$ is generated, $b_{\text{in}}(\omega)$ can be set to zero. Therefore the transmission fit function in this case is given by

$$S_{21}(\omega) = T_0 e^{i\phi} \frac{b_{\text{out}}(\omega)}{a_{\text{in}}(\omega)} = T_0 e^{i\phi} \frac{\sqrt{\kappa_{\text{in}}\kappa_{\text{out}}}}{\frac{\gamma + \kappa_{\text{in}} + \kappa_{\text{out}}}{2} - i(\omega - \omega_1)} \tag{21}$$

where T_0 is a parameter to fit the maximum transmission amplitude and ϕ is an arbitrary phase.

The same derivation of the fit function can now be done for other compositions, using the corresponding Hamiltonian H_{sys}.

2.2.1 Coupling to Purcell filter

The corresponding Hamiltonian to the model in figure 5 is

$$H_{\text{sys}} = \hbar\omega_1 A^\dagger A + \hbar\omega_2 B^\dagger B + \hbar\omega_3 C^\dagger C + \hbar J_2 (A^\dagger B + B^\dagger A) + \hbar J_3 (A^\dagger C + C^\dagger A) \tag{22}$$

with the commutators

$$[A(t), H_{\text{sys}}] = \hbar\omega_1 A(t) + \hbar J_2 B(t) + \hbar J_3 C(t) \tag{23a}$$

$$[B(t), H_{\text{sys}}] = \hbar\omega_2 B(t) + \hbar J_2 A(t) \tag{23b}$$

$$[C(t), H_{\text{sys}}] = \hbar\omega_3 C(t) + \hbar J_3 A(t) \tag{23c}$$

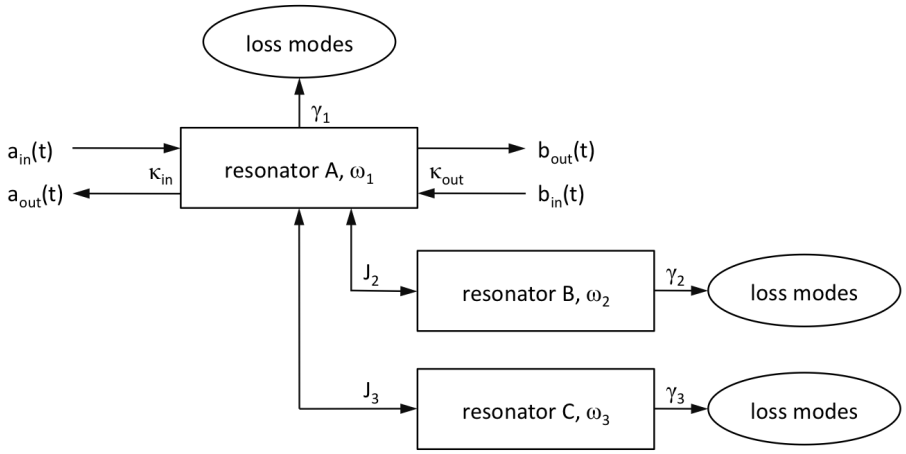

Figure 5: Schematic of the input-output model of two quarter-wavelength resonators (B, C) coupled to a Purcell filter (A).

Inserting these commutation relations in the Heisenberg equations of motion and applying Fourier transformation yields the following system of equations:

$$\left(-i(\omega-\omega_1)+\frac{\kappa_{\text{in}}+\kappa_{\text{out}}+\gamma_1}{2}\right)A(\omega)=-iJ_2B(\omega)-iJ_3C(\omega)+\sqrt{\kappa_{\text{in}}}a_{\text{in}}(\omega)+\sqrt{\kappa_{\text{out}}}b_{\text{in}}(\omega) \tag{24a}$$

$$\left(-i(\omega-\omega_2)+\frac{\gamma_2}{2}\right)B(\omega)=-iJ_2A(\omega) \tag{24b}$$

$$\left(-i(\omega-\omega_3)+\frac{\gamma_3}{2}\right)C(\omega)=-iJ_3A(\omega) \tag{24c}$$

$$a_{\text{in}}(\omega)+a_{\text{out}}(\omega)=\sqrt{\kappa_{\text{in}}}A(\omega) \tag{24d}$$

$$b_{\text{in}}(\omega)+b_{\text{out}}(\omega)=\sqrt{\kappa_{\text{out}}}A(\omega) \tag{24e}$$

Solving this system of equations for $b_{\text{in}}(\omega)=0$ yields the transmission fit function analogous to equation (21):

$$S_{21}(\omega)=T_0e^{i\phi}\frac{\sqrt{\kappa_{\text{in}}\kappa_{\text{out}}}}{\frac{\gamma_1+\kappa_{\text{in}}+\kappa_{\text{out}}}{2}-i(\omega-\omega_1)+\frac{J_2^2}{\gamma_2/2-i(\omega-\omega_2)}+\frac{J_3^2}{\gamma_3/2-i(\omega-\omega_3)}} \tag{25}$$

Note that the only difference to equation (21) are the two additive terms in the denominator which correspond to the coupling of resonator B and C to the resonator A. In the case where only one resonator is coupled to the Purcell filter, the same derivation leads to the fit function:

$$S_{21}(\omega)=T_0e^{i\phi}\frac{\sqrt{\kappa_{\text{in}}\kappa_{\text{out}}}}{\frac{\gamma_1+\kappa_{\text{in}}+\kappa_{\text{out}}}{2}-i(\omega-\omega_1)+\frac{J_2^2}{\gamma_2/2-i(\omega-\omega_2)}} \tag{26}$$

2.2.2 Coupling to transmission line

The corresponding Hamiltonian to the model in figure 6 is

$$H_{\text{sys}}=\hbar\omega_1A^\dagger A+\hbar\omega_2B^\dagger B+\hbar\omega_3C^\dagger C \tag{27}$$

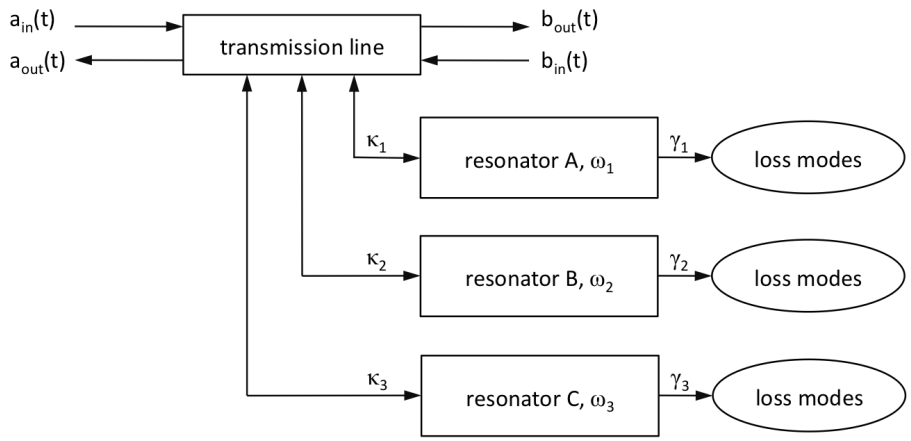

Figure 6: Schematic of the input-output model of three quarter-wavelength resonators coupled to a transmission line.

which leads to the following system of equations:

$$\left(-i(\omega-\omega_1)+\frac{\kappa_1+\gamma_1}{2}\right)A(\omega)=\sqrt{\kappa_1}\left(a_{\mathrm{in}}(\omega)+b_{\mathrm{in}}(\omega)\right) \tag{28a}$$

$$\left(-i(\omega-\omega_2)+\frac{\kappa_2+\gamma_2}{2}\right)B(\omega)=\sqrt{\kappa_2}\left(a_{\mathrm{in}}(\omega)+b_{\mathrm{in}}(\omega)\right) \tag{28b}$$

$$\left(-i(\omega-\omega_3)+\frac{\kappa_3+\gamma_3}{2}\right)C(\omega)=\sqrt{\kappa_3}\left(a_{\mathrm{in}}(\omega)+b_{\mathrm{in}}(\omega)\right) \tag{28c}$$

$$a_{\mathrm{in}}(\omega)-a_{\mathrm{out}}(\omega)+b_{\mathrm{in}}(\omega)-b_{\mathrm{out}}(\omega)=\sqrt{\kappa_1}A(\omega)+\sqrt{\kappa_2}B(\omega)+\sqrt{\kappa_3}C(\omega) \tag{28d}$$

$$a_{\mathrm{in}}(\omega)+a_{\mathrm{out}}(\omega)=b_{\mathrm{in}}(\omega)+b_{\mathrm{out}}(\omega) \tag{28e}$$

Note that this model assumes independent resonators A, B and C which is only granted if the resonance frequencies are sufficiently separated. Solving this system of equations for $b_{\mathrm{in}}(\omega)=0$ leads to the transmission fit function:

$$S_{21}(\omega)=T_0e^{i\phi}\left(1-\frac{\kappa_1}{\kappa_1+\gamma_1-2i(\omega-\omega_1)}-\frac{\kappa_2}{\kappa_2+\gamma_2-2i(\omega-\omega_2)}-\frac{\kappa_3}{\kappa_3+\gamma_3-2i(\omega-\omega_3)}\right) \tag{29}$$

3 Samples and measurement setup

In this section, the different sample designs and their measurement are described. Since the simulation of the samples is another important part of the results, it is discussed as well. The fabrication of the devices was not part of the project, therefore the fabrication process is not described here. All measured devices are made from niobium on a sapphire substrate. Niobium has a critical temperature of $T_c = 9.2\,\mathrm{K}$ which allows to perform measurements in liquid helium ($T = 4.2\,\mathrm{K}$).

3.1 Device details and measurement

The first device depicted in figure 7a contains two symmetrically coupled half-wavelength resonators with different resonance frequencies, but with the same coupling capacitances $C_\kappa = 0.3\,\mathrm{fF}$. The second device is similar, but with another coupling capacitance $C_\kappa = 0.9\,\mathrm{fF}$. In both cases, the coupling capacitor is a small gap in the transmission line before the ports. These samples are measured to test a new wafer.

The third device shown in figure 7b contains two quarter-wavelength resonators used as Purcell filters with input coupling capacitances $C_\kappa = 9\,\mathrm{fF}$. The one at the left hand side between port 1 and 2 is coupled to two other quarter-wavelength resonators which is schematically shown in figure 5. The other resonator at the right hand side between 3 and 4 has a higher resonance frequency and is only coupled to one other quarter-wavelength resonator. The Purcell filters which are coupled to the qubit readout resonators protect the qubit from decay. This sample is measured to characterize the coupling of readout resonators to Purcell filter.

The fourth device depicted in figure 7c consists of a transmission line which is interrupted by a finger capacitor at the left hand side and three quarter-wavelength resonators coupled to it. The ground plane width between the resonators and the transmission line is 8 µm. This sample is measured to characterize the coupling of quarter-wavelength resonators to a transmission line open at one end which has the advantage of unlimited coupling length.

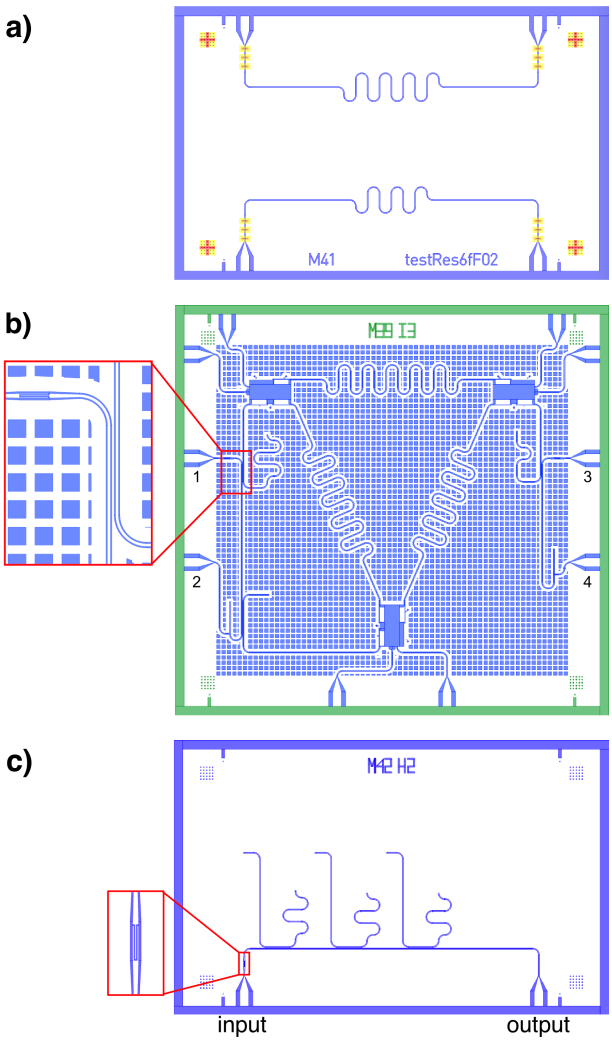

Figure 7: Different measured devices. a) Half-wavelength resonators. b) Quarter-wavelength resonators coupled to Purcell filter. c) Quarter-wavelength resonators coupled to transmission line with input capacitor.

For the measurement, the samples are mounted on a printed circuit board (PCB). The PCB is then fixed on a sample holder and connected to the dipstick via SMP connectors. For the samples in figure 7a and 7c a 8-port dipstick is used, whereas for the sample in figure 7b a 16-port dipstick is needed. The dipstick is inserted in a dewar containing liquid helium. The ports of the dipstick are connected to the vector network analyzer (VNA) which performs a S-parameter measurement. The samples in figure 7a and 7b are measured in a four-port measurement and the sample in figure 7c in a two-port measurement. Before the measurement can start, the VNA has to be calibrated which is done electrically. The calibration included the cables from the VNA to the dipstick, but not the dipstick itself. For the measurement the following settings are chosen:

- input power: $0.0\,\mathrm{dBm} \mathrel{\widehat{=}} 1\,\mathrm{mW}$
- IF bandwidth: 50 kHz
- average factor: 500 (20 for calibration)

- frequency: 300 kHz - 20 GHz
- points: 20'000

The spectrum is saved for further analysis in *Mathematica*. The dipstick is taken out of the dewar carefully and then heated with an air blower before the sample can be removed.

3.2 Simulation

In order to understand the dependencies of the resonator on different parameters, the investigated designs are also simulated in *AWR Microwave Office*. The transmission lines (TLIN) are represented by elements with a characteristic impedance Z0 and a certain electrical length (EL) which represents the phase shift that the field at center frequency F0 obtains while travelling through the transmission line. A quarter-wavelength resonator for example can be simulated by this element using an electrical length of 90°. Other used elements are capacitors CAP with capacitance C and ports with impedance Z.

To see how the circuit behave, a S-parameter measurement between port 1 and 2 is simulated and visualized. The different parameters can then be changed and the result is directly visible. The simulated data is then exported for comparison with the theoretical fit model in *Mathematica*.

In order to design the preferred coupling capacitances between readout resonators and transmission line, line coupler with different coupling lengths were already simulated in *Sonnet* for separation gaps of 5 and 10 µm between transmission line and readout resonator. These simulations are used to plot the coupling capacitance as a function of coupling length.

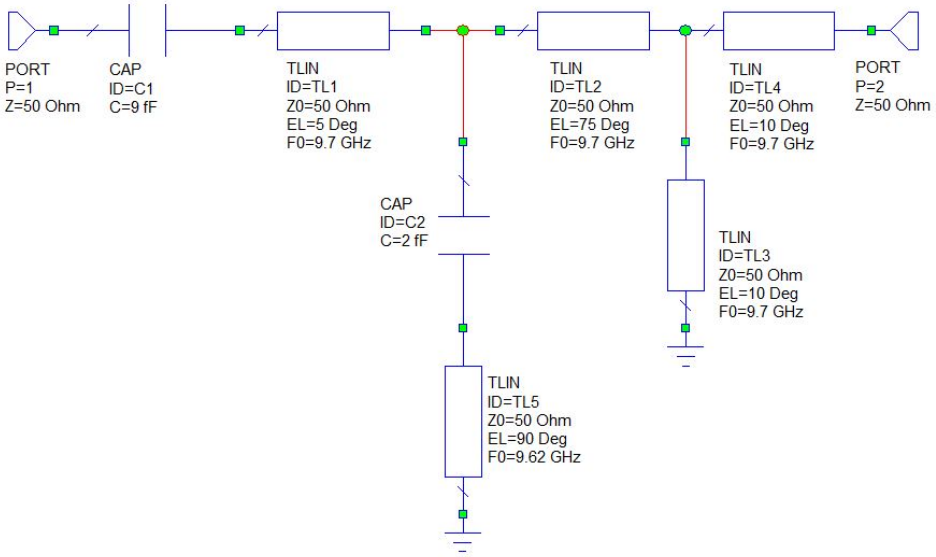

Figure 8: Circuit for simulation of the third device in *AWR Microwave Office*. One quarter-wavelength resonator (TL5) is coupled to the quarter-wavelength Purcell filter.

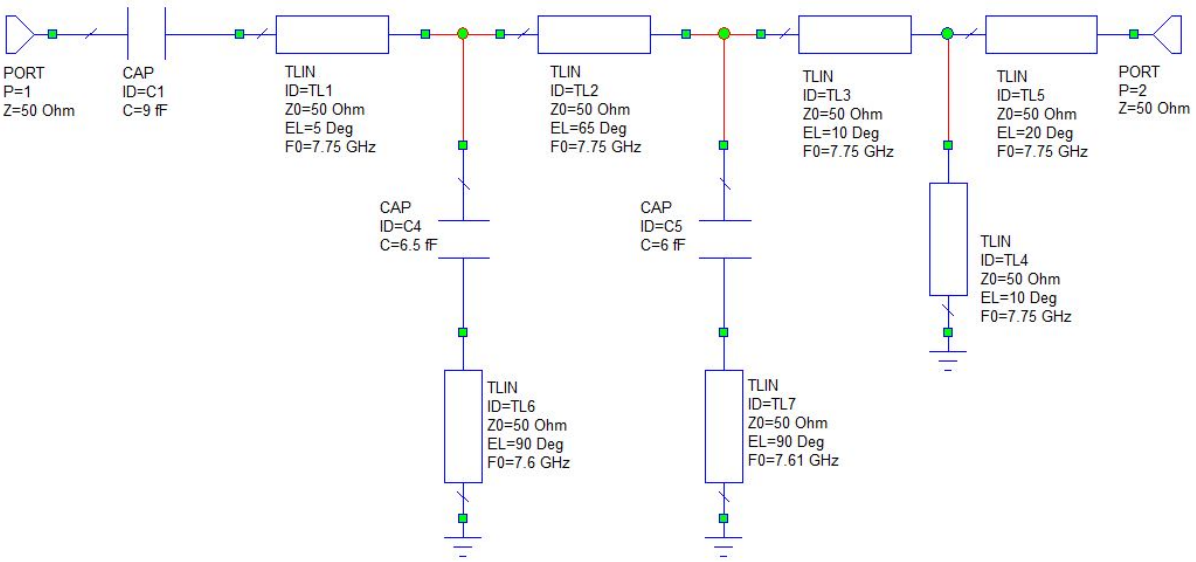

Figure 9: Circuit for simulation of the third device in *AWR Microwave Office*. This circuit corresponds to the schematic in figure 5. Two quarter-wavelength resonators (TL6 and TL7) are coupled to the quarter-wavelength Purcell filter.

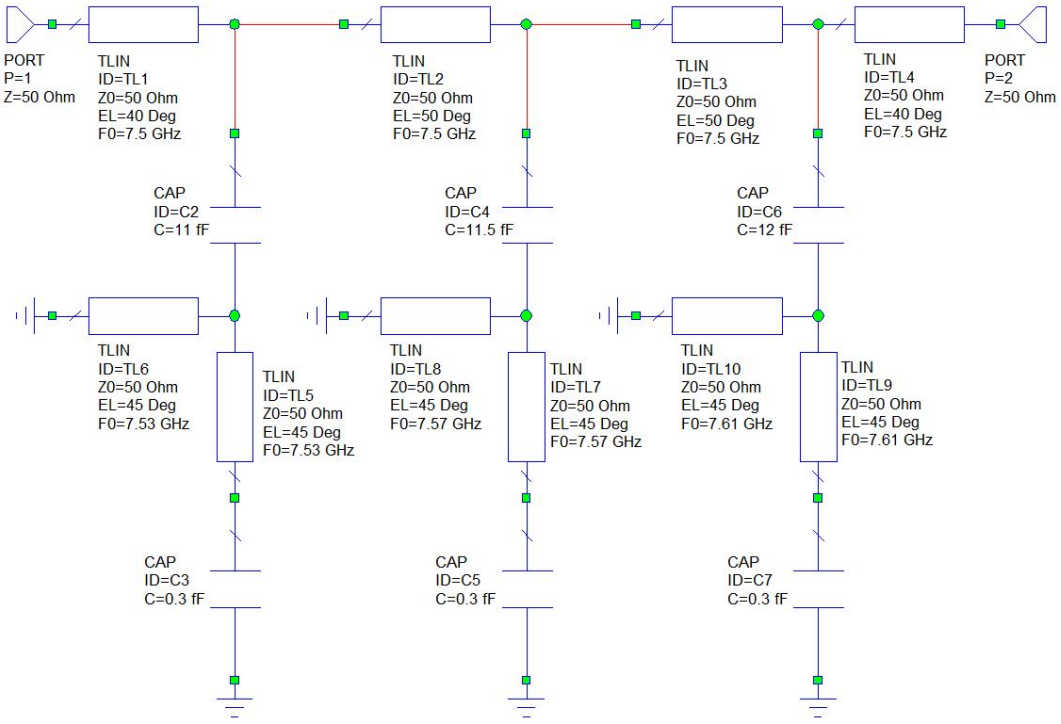

Figure 10: Circuit for simulation of three quarter-wavelength resonators (TL5 to TL10) coupled to transmission line (TL1 to TL4) in *AWR Microwave Office*. In contrast to the fourth measured device, there is no input capcitor in the transmission line. This circuit corresponds to the schematic in figure 6.

4 Results and discussion

The following subsections show the results of the measurement and the simulation of the different samples. There are always three plots from which the first plot shows the modulus of the transmission amplitude in dB, the second plot reveals the real and the imaginary part of the

amplitude as a function of frequency and the third plot represents the phase as the imaginary part versus the real part of the amplitude is plotted. The black curve shows the calculated function from section 2 fitted to the data with "NonlinearModelFit" in *Mathematica*.

4.1 Half-wavelength resonator

The data for the single half-wavelength resonators is fitted using the function (21) derived in section 2. Figure 11 shows the measured and fitted data of the symmetrically coupled half-wavelength resonators with coupling capacitances $C_\kappa = 0.3\,\mathrm{fF}$.
Figure 12 shows the measured and fitted data of the symmetrically coupled half-wavelength resonators with coupling capacitances $C_\kappa = 0.9\,\mathrm{fF}$.

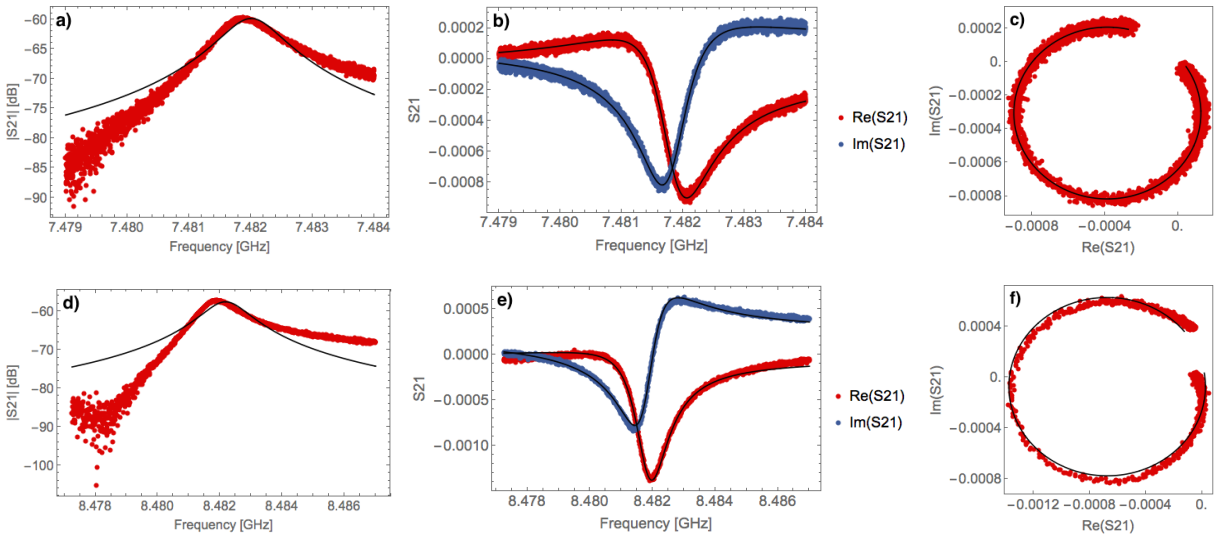

Figure 11: Measured transmission of sample 1 (see figure 7a): symmetrically coupled single half-wavelength resonators with coupling capacitances $C_\kappa = 0.3\,\mathrm{fF}$ and resonance frequencies $f_0 = 7.5\,\mathrm{GHz}$ (a - c) and $8.5\,\mathrm{GHz}$ (d - f).

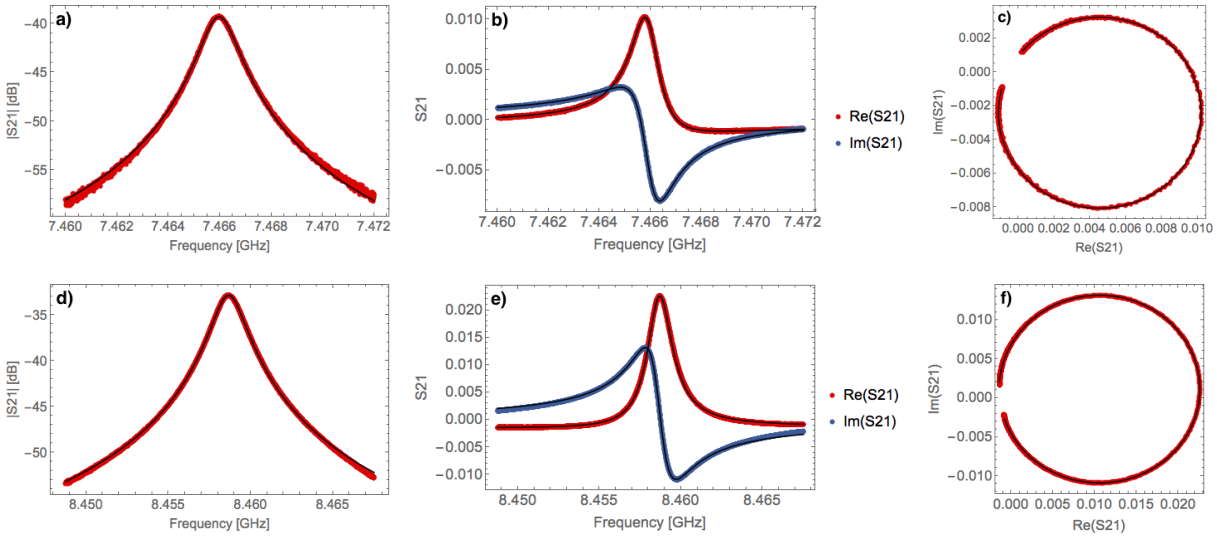

Figure 12: Measured transmission of sample 2 (see figure 7a): symmetrically coupled single half-wavelength resonators with coupling capacitances $C_\kappa = 0.9\,\mathrm{fF}$ and resonance frequencies $f_0 = 7.5\,\mathrm{GHz}$ (a - c) and $8.5\,\mathrm{GHz}$ (d - f).

C_κ [fF]	f_0 [GHz]	$\kappa/2\pi$ [MHz]	Q_L	Q_int	Q_ext
0.3	7.482	1.0	7.7×10^3	7.7×10^3	7.5×10^6
0.3	8.482	1.3	6.7×10^3	6.7×10^3	4.8×10^6
0.9	7.466	1.4	5.4×10^3	5.5×10^3	4.8×10^5
0.9	8.464	1.3	6.5×10^3	6.6×10^3	3.8×10^5

Table 1: Results from the measurement of the first two samples. The half-wavelength resonators are symmetrically coupled with capacitance C_κ.

The values show that for the higher coupling capacitance, the resonance frequency decreases. Further, κ increases which leads to a decrease of the loaded quality factor.
From theory it is expected that κ of an undercoupled resonator is independent of the coupling capacitance whereas κ of a resonator in the overcoupled regime depend on the coupling capacitance as well as on the resonance frequency (see eq. (9) and (10)). The measurement of the first two devices shows that they are in the undercoupled regime, so κ is almost independent of the coupling capacitance (see table 1).
Since the attenuation constant α is unknown, the values for κ can not be calculated from theory, but in reverse, the measured values lead with equation (9) to $\alpha \approx 2.6(5) \times 10^{-2}\,\mathrm{m}^{-1}$.

4.2 Quarter-wavelength resonators coupled to Purcell filter

The measurement and simulation results of the quarter-wavelength resonator coupled to Purcell filter at $f_0 = 9.5\,\mathrm{GHz}$ are shown in figure 13. The data is fitted with the function (26) in section 2.

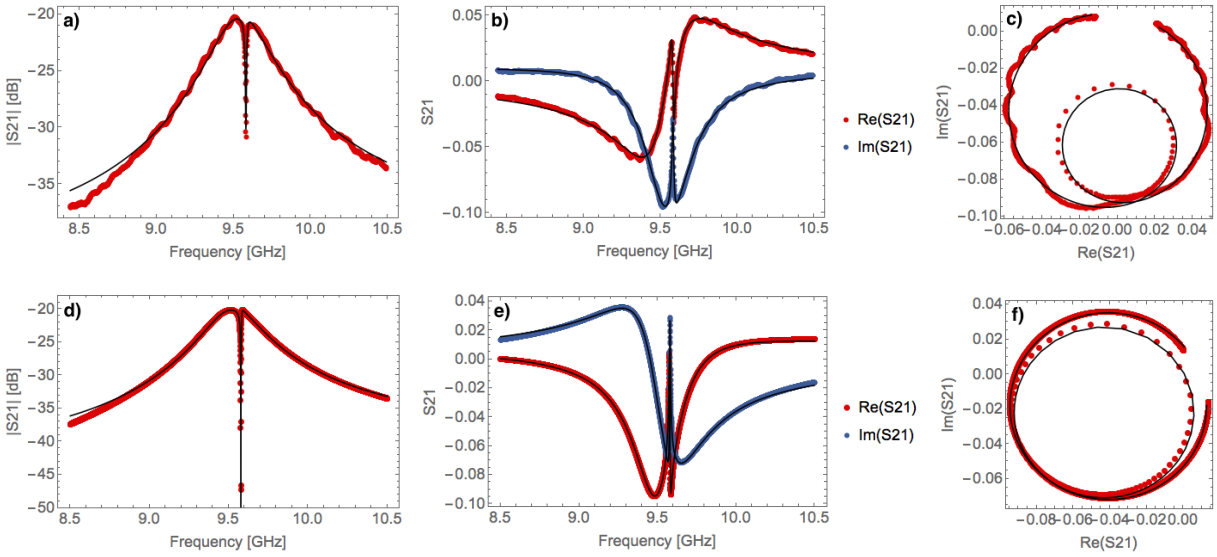

Figure 13: (a-c) Measured and (d-f) simulated transmission of sample 3 (see figure 7b): one quarter-wavelength resonator (B) coupled to a Purcell filter (A) with center frequency $f_0 = 9.5\,\mathrm{GHz}$ and input capacitance $C_\mathrm{in} = 9\,\mathrm{fF}$.

	$f_{0,\mathrm{A}}$ [GHz]	$\kappa_\mathrm{A}/2\pi$ [MHz]	$f_{0,\mathrm{B}}$ [GHz]	$\kappa_\mathrm{B}/2\pi$ [MHz]	$J_\mathrm{B}/2\pi$ [MHz]
Measurement	9.539	353	9.580	10	31
Simulation	9.522	382	9.583	12	35

Table 2: Results from the measurement and simulation of the third sample. The quarter-wavelength resonator B is coupled to a quarter-wavelength resonator A. Resonator A is used as a Purcell filter with input capacitance $C_\mathrm{in} = 9\,\mathrm{fF}$.

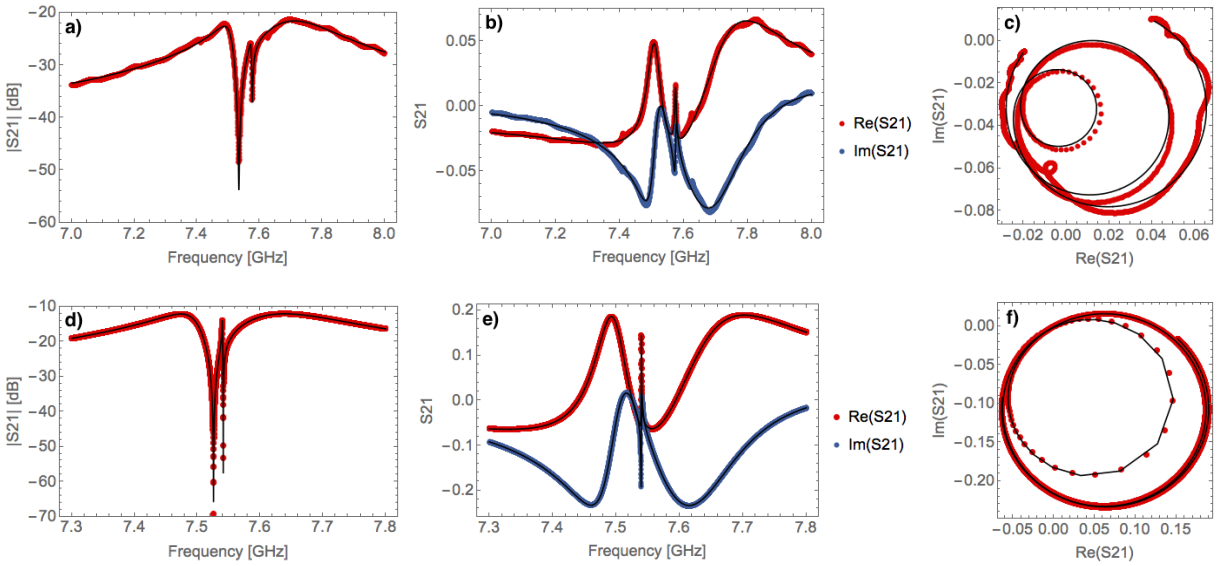

Figure 14: (a-c) Measured and (d-f) simulated transmission of sample 3 (see figure 7b): two quarter-wavelength resonators (B and C) coupled to a Purcell filter (A) with $f_0 = 7.5\,\mathrm{GHz}$ and input capacitance $C_{\mathrm{in}} = 9\,\mathrm{fF}$.

	$f_{0,\mathrm{A}}$ [GHz]	$\kappa_{\mathrm{A}}/2\pi$ [MHz]	$f_{0,\mathrm{B}}$ [GHz]	$\kappa_{\mathrm{B}}/2\pi$ [MHz]	$J_{\mathrm{B}}/2\pi$ [MHz]	$f_{0,\mathrm{C}}$ [GHz]	$\kappa_{\mathrm{C}}/2\pi$ [MHz]	$J_{\mathrm{C}}/2\pi$ [MHz]
Measurement	7.665	251	7.533	48	79	7.576	8.3	28
Simulation	7.583	218	7.524	75	72	7.541	8.3	23

Table 3: Results from the measurement and simulation of the third sample. The quarter-wavelength resonators B and C are coupled to a quarter-wavelength resonator A. Resonator A with input capacitance $C_{\mathrm{in}} = 9\,\mathrm{fF}$ is used as a Purcell filter.

The measurement and simulation results of the two quarter-wavelength resonators coupled to Purcell filter at $f_0 = 7.5\,\mathrm{GHz}$ on sample 3 are shown in figure 14. The data is fitted with the function (25) in section 2.

The transmission spectrum from the third measured device shows the Lorentzian shape from the Purcell filter. In the case where one resonator at $f_0 = 9.5\,\mathrm{GHz}$ is coupled, there is one dip at the resonance frequency. In the case of two resonators coupled at $f_0 = 7.5\,\mathrm{GHz}$, there are two dips. The two resonance frequencies are too close or the coupling strength too big which leads to the merged dips. The simulated results are similar to the measured ones. It has to be mentioned that for simplicity, the quarter-wavelength resonators are assumed to be coupled at the open end in the simulation. Therefore, the coupling capacitances in the simulation do not match with the ones on the device.
The results show that the Purcell filter only offers limited bandwidth for the coupling of readout resonators. An even bigger problem for multiplexing readout is the limited physical length of the Purcell filter which makes it difficult to use it for coupling several readout resonators to it.

4.3 Quarter-wavelength resonators coupled to transmission line open at one end

In figure 15, the measured data of the fourth sample is shown. The dip in the middle is hardly visible. Due to the small dips and the relative big influence of impedance mismatch in the transmission line, the data is not fitted to the theoretical model.

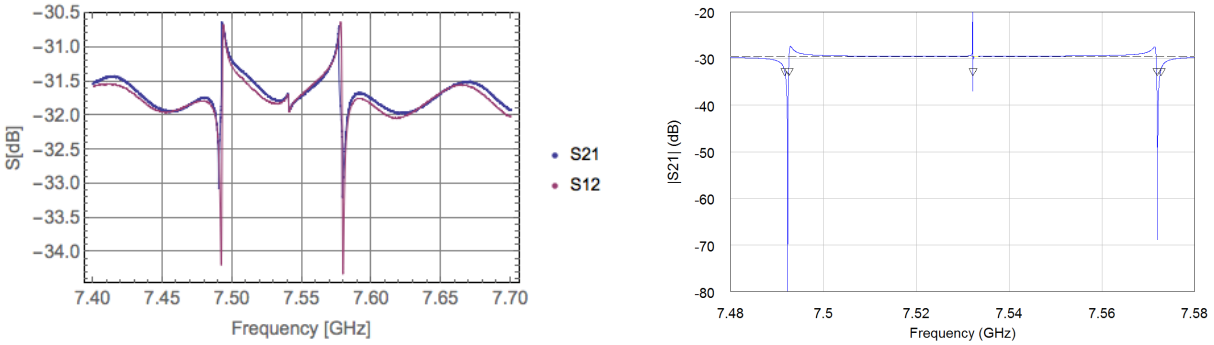

(a) Measurement (b) Simulation

Figure 15: Transmission of sample 4 (see figure 7c): three quarter-wavelength resonators coupled to a transmission line which is coupled to the input port with a capacitor.

The measurement of the fourth device shows that due to the input capacitor in the transmission line, there is a standing wave which can cause very weakly coupling to the resonator, if the coupling position is in a node of the standing wave.

4.4 Quarter-wavelength resonators coupled to transmission line

To get rid of the standing wave in the transmission line which causes different coupling strength for different positions within the transmission line, the quarter-wavelength resonators are simulated to be coupled to a transmission line without input capacitor. The desired values for $\kappa/2\pi$ are between 1.5 MHz and 2 MHz. Therefore, the capacitances and the coupling position within the resonators have to be chosen appropriately. The results of this simulation and the fit curve are shown in figure 16.
The coupling strength of the resonator coupled to the transmission line depends on the coupling position within the resonator. If $\kappa_{\max}$ describes the coupling strength (for the formula see eq. (13)) at the open end of the quarter-wavelength resonator, the coupling strength $\kappa(l)$ for coupling at a position of distance l away from the open end is smaller. From *Microwave Office* simulation of capacitively coupling, it can be assumed: $\kappa(l) \approx \kappa_{\max} \cos^2(2\pi l/\lambda)$ (see figure 17).

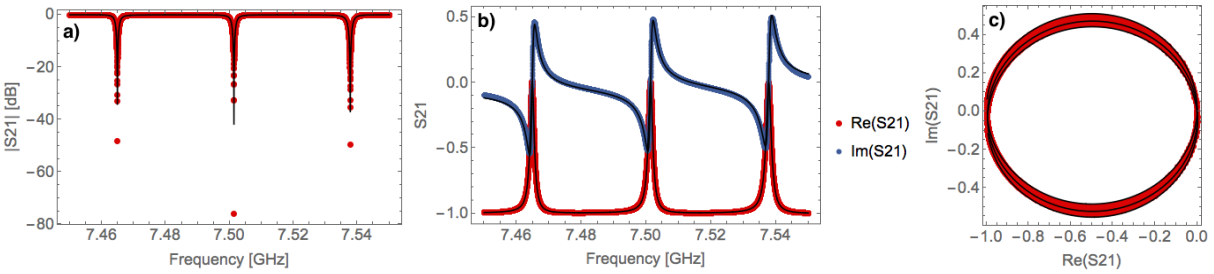

Figure 16: Simulated transmission of three quarter-wavelength resonators coupled to transmission line. The corresponding circuit schematic is shown in figure 10. The resonators are assumed to be coupled in their middles (EL = 45° from the open end) to the transmission line with coupling capacitances $C_{\kappa,\mathrm{A}} = 11\,\mathrm{fF}$, $C_{\kappa,\mathrm{B}} = 11.5\,\mathrm{fF}$ and $C_{\kappa,\mathrm{C}} = 12\,\mathrm{fF}$

$f_{0,\mathrm{A}}$ [GHz]	$\kappa_{\mathrm{A}}/2\pi$ [MHz]	$f_{0,\mathrm{B}}$ [GHz]	$\kappa_{\mathrm{B}}/2\pi$ [MHz]	$f_{0,\mathrm{C}}$ [GHz]	$\kappa_{\mathrm{C}}/2\pi$ [MHz]
7.465	1.52	7.501	1.65	7.538	1.94

Table 4: Results from the simulation of three quarter-wavelength resonators coupled to transmission line.

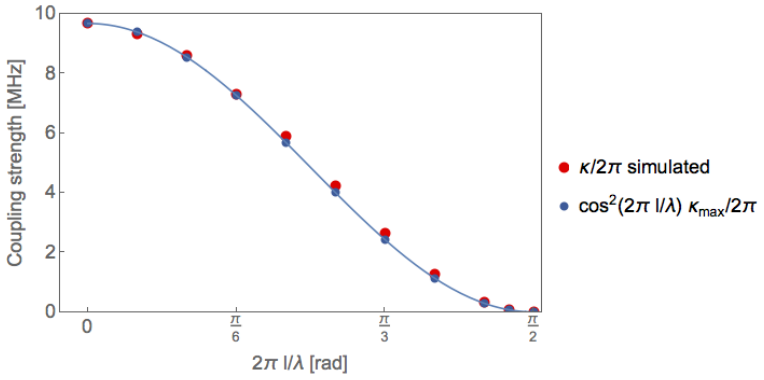

Figure 17: Comparison of simulated values for $\kappa/2\pi$ with the values calculated by $\cos^2(2\pi l/\lambda)\kappa_{\max}/2\pi$ for different coupling positions of the quarter-wavelength resonator coupled with capacitance $C_\kappa = 20\,\mathrm{fF}$ to transmission line. Here, the length l indicates the distance between the coupling position and the open end of the quarter-wavelength resonator.

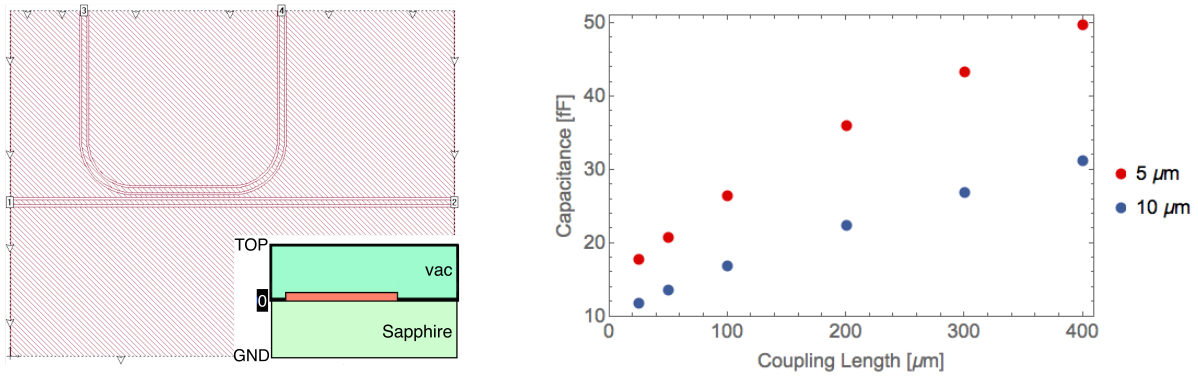

(a) (b)

Figure 18: (a) *Sonnet* simulation for a coupling length of 200 µm. (b) Simulated coupling capacitances at $f_0 = 7.5\,\mathrm{GHz}$ for different coupling lengths in the cases of 5 µm and 10 µm separation gap (width of ground plane between the center conductors).

The expected coupling capacitances are simulated with *Sonnet*. In figure 18 (b) the simulated capacitances for $f_0 = 7.5\,\mathrm{GHz}$ are shown as a function of the coupling length.

5 Conclusion and Outlook

To build more complex on-chip circuits with several qubits, it is necessary to have a multiplexing readout design. The coupling of several readout resonators to a Purcell filter, which would prevent the qubit from decay, is not possible due to the limited coupling length and the limited bandwith. The coupling to a transmission line with input capacitance seemed to be an option. The reason for putting the input capacitor is the fact, that the signal is reflected at the capacitor and can therefore be detected at only one port. However, the measurement of sample 4 showed that this is no option because the standing wave in the transmission line caused by the input capacitor would require well calculated coupling positions for the readout resonators which is in fact hardly possible to design. Hence it is proposed to couple the readout resonators to a bare transmission line connecting two ports. This is adapted in the current designing process.
Since the suggested design does not use Purcell filter, the qubit is not protected from decay. This problem has to be solved by a new type of filter which is proposed in [1].

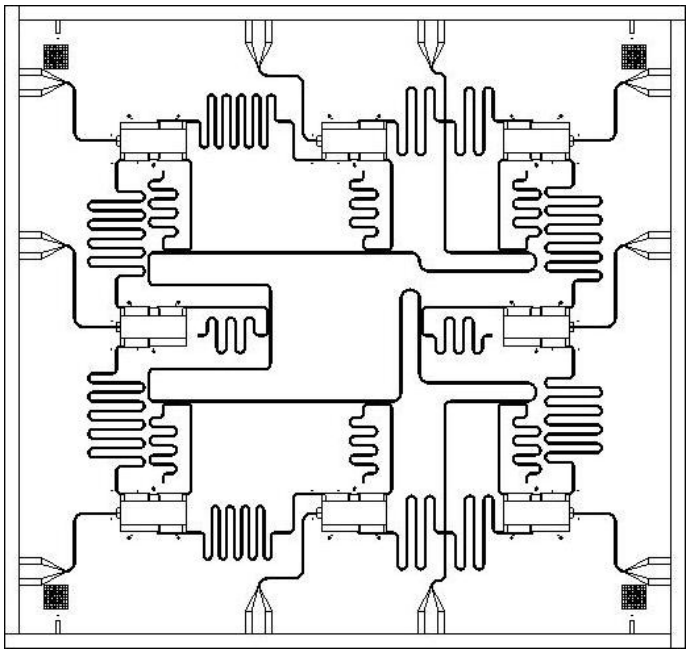

Figure 19: Design for multiplexing qubit readout. The transmission line between the top right and the bottom right port is capacitively coupled to eight qubit readout resonators.

Beside the measurement of the devices, the derivation of fit functions for the transmission spectrum for the investigated circuits and their implementation in *Mathematica* was an important part of the project. The fitting routines used at the beginning were quite inefficient and the created plots did not show what was really fitted. This was improved before using the program to fit the data.

In order to determine the coupling strength and other resonator properties more precisely, the different parameters of the design, like the attenuation constant α, the effective permittivity ε_{eff} and the coupling capacitance per unit length of the transmission line C_l have to be known more exactly.

6 Acknowledgement

I thank Prof. Dr. Andreas Wallraff for giving me the opportunity to conduct my Semester thesis at the Quantum Device Lab. Furthermore, I would like to thank my supervisor Dr. Mintu Mondal for introducing me to the topic and the software. He was always ready to answer my questions.

References

[1] N. T. Bronn, E. Magesan, N. A. Masluk, J. M. Chow, J. M. Gambetta, and M. Steffen. "Reducing Spontaneous Emission in Circuit Quantum Electrodynamics by a Combined Readout/Filter Technique." arXiv:1504.04353 [quant-ph] (2015).

[2] L. Frunzio, A. Wallraff, D. Schuster, J. Majer, and R. Schoelkopf. "Fabrication and Characterization of Superconducting Circuit QED Devices for Quantum Computation." *IEEE Trans. Appl. Supercond.* **15**, 860 (2005).

[3] M. Göppl, A. Fragner, M. Baur, R. Bianchetti, S. Filipp, J. M. Fink, P. J. Leek, G. Puebla, L. Steffen, and A.Wallraff. "Coplanar waveguide resonators for circuit quantum electrodynamics." *Journal of Applied Physics* **104**, 113904 (2008).

[4] G. Hammer, S. Wuensch, K. Ilin and M. Siegel. "Ultra high quality factor resonators for kinetic inductance detectors." *Journal of Physics: Conference Series* **97**, 012044 (2008).

[5] W. Hayt and J. Buck, *Engineering Electromagnetics.* New York, USA: McGraw-Hill, 2012.

[6] R. J. Schoelkopf and S. M. Girvin. "Wiring up quantum systems." *Nature* **451**, 664-669 (2008).

[7] L. Steffen, *Quantum Teleportation and Efficient Process Verification with Superconducting Circuits.* Ph.D. thesis, ETH Zürich (2013).

[8] D. F. Walls and G. J. Milburn, *Quantum Optics.* Berlin, Germany: Springer-Verlag, 2008.

[9] F. Winterer, *Characterization of the Linear Response and the Tunability of Two Coupled LC Oscillators.* Semester thesis, ETH Zürich (2013).

ETH

Eidgenössische Technische Hochschule Zürich
Swiss Federal Institute of Technology Zurich

Declaration of originality

The signed declaration of originality is a component of every semester paper, Bachelor's thesis, Master's thesis and any other degree paper undertaken during the course of studies, including the respective electronic versions.

Lecturers may also require a declaration of originality for other written papers compiled for their courses.

I hereby confirm that I am the sole author of the written work here enclosed and that I have compiled it in my own words. Parts excepted are corrections of form and content by the supervisor.

Title of work (in block letters):

Characterization of microwave devices for multiplexing qubit readout.

Authored by (in block letters):

For papers written by groups the names of all authors are required.

Name(s):	**First name(s):**
Caspar	Patrik

With my signature I confirm that

- I have committed none of the forms of plagiarism described in the 'Citation etiquette' information sheet.
- I have documented all methods, data and processes truthfully.
- I have not manipulated any data.
- I have mentioned all persons who were significant facilitators of the work.

I am aware that the work may be screened electronically for plagiarism.

Place, date	**Signature(s)**
Zürich, 20.07.2015	P. Caspar

For papers written by groups the names of all authors are required. Their signatures collectively guarantee the entire content of the written paper.